

Dissipative Kerr Solitons in a III-V Microresonator

Gregory Moille,^{1,2,*} Lin Chang,^{3,*} Weiqiang Xie,^{3,*} Ashutosh Rao,^{1,4} Xiyuan Lu,^{1,4} Marcelo Davanco,¹ John E. Bowers,^{3,†} and Kartik Srinivasan^{1,2,‡}

¹*Microsystems and Nanotechnology Division, National Institute of Standards and Technology, Gaithersburg, USA*

²*Joint Quantum Institute, NIST/University of Maryland, College Park, USA*

³*Department of Electrical and Computer Engineering, University of California, Santa Barbara, USA*

⁴*Institute for Research in Electronics and Applied Physics and Maryland Nanocenter, University of Maryland, College Park, USA*

(Dated: December 22, 2024)

We demonstrate stable microresonator Kerr soliton frequency combs in a III-V platform (Al-GaAs on SiO₂) through quenching of thermorefractive effects by cryogenic cooling to temperatures between 4 K and 20 K. This cooling reduces the resonator's thermorefractive coefficient, whose room-temperature value is an order of magnitude larger than that of other microcomb platforms like Si₃N₄, SiO₂, and AlN, by more than two orders of magnitude, and makes soliton states adiabatically accessible. Realizing such phase-stable soliton operation is critical for applications that fully exploit the ultra-high effective nonlinearity and high optical quality factors exhibited by this platform.

Microresonator frequency combs based on dissipative Kerr solitons (DKSs) [1] are promising for chip-scale metrology implementation, including applications such as optical clocks [2, 3], spectroscopy systems [4], and range measurements [5]. DKSs have been demonstrated in amorphous dielectrics such as SiO₂ [6] and Si₃N₄ [7], crystalline materials such as MgF₂ [8], III-Nitride materials such as AlN [9, 10], and promising new integrated photonics platforms such as thin film LiNbO₃ [11]. In contrast, III-As materials, though they are particularly attractive for microcomb applications due to the ability to simultaneously realize ultra-high effective nonlinearity [12] and large optical quality factor [13, 14], are yet to show stable microcavity DKS operation. Given the competing processes that can occur in such materials, including thermorefractive, free carrier, and photorefractive effects, achieving this milestone is important to further establish the potential of these platforms for applications that require phase-stable frequency comb generation.

III-V materials, mostly binary or ternary compounds made of Aluminum (Al), Gallium (Ga), Arsenic (As) and Phosphorus (P), started to gain attention more than three decade ago for photonics applications thanks to their large third-order nonlinearity [15, 16] - two-to-three orders of magnitude higher than SiO₂ [17], Si₃N₄ [17] and AlN [18] - and the avoidance of two-photon absorption (TPA) in the telecom band [19] thanks to band-gap engineering [20]. Reduction in TPA resulted in several milestones for nonlinear photonics such as waveguide soliton pulse compression in suspended GaAs photonic crystal membranes [21], energy-efficient optical gates [22, 23], and ultra-low threshold optical parameter oscillators [24]. A major breakthrough has been the emergence of the

III-V on insulator platform [12], which has helped address longstanding challenges with respect to scattering losses [25, 26], and resulted in the realization of high quality factor ($Q > 10^6$) microring resonators [13, 14] in which geometric dispersion control can be exercised. Together with the ultra-high effective nonlinearity, these devices have achieved comb generation at pump powers easily reachable with chip-integrated lasers [13]. However, while a transient 'soliton step' was observed in Ref. [13], indicating soliton existence, stable access and operation on a DKS state was not achieved in that work.

Here, we demonstrate the first stable generation of DKSs in a III-V microresonator. The DKS is thermally accessible under manual tuning of the pump laser frequency, due to a dramatic drop in the thermorefractive coefficient ($\partial n/\partial T$, where n is the system's refractive index and T is temperature) realized by a cryogenic operating temperature ($T < 20$ K). We measure the system's temperature-dependent $\partial n/\partial T$ and show that its large gradient creates a limited window for which DKSs are thermally accessible. Within this range there is a balance between high enough power to sustain the DKS and low enough power to avoid strong heating that increases the resonator's thermorefractive coefficient and reduces the DKS accessibility region (i.e., shortens the DKS step length).

The experimental setup (Fig. 1) is similar to ref. [27], where the sample is in a 20 cm diameter closed-cycle cryostat whose sample mount temperature can be set from 4 K to 100 K. The resonator is a microring of radius $R = 18.97 \mu\text{m}$ and ring width $RW = 740$ nm, made in 400 nm thick Al_{0.2}Ga_{0.8}As encapsulated in SiO₂ [13]. The microring chip is accessed by lensed optical fibers (insertion loss of 6 dB/facet), and is pumped by an amplified continuous tunable laser (CTL). The resonator output spectrum is monitored with an optical spectrum analyzer (OSA), and a second CTL is used in heterodyne beat note measurements against the generated comb, detected by a 12 GHz photodiode and an electrical spectral analyzer.

* These authors contributed equally

† bowers@ece.ucsb.edu

‡ kartik.srinivasan@nist.gov

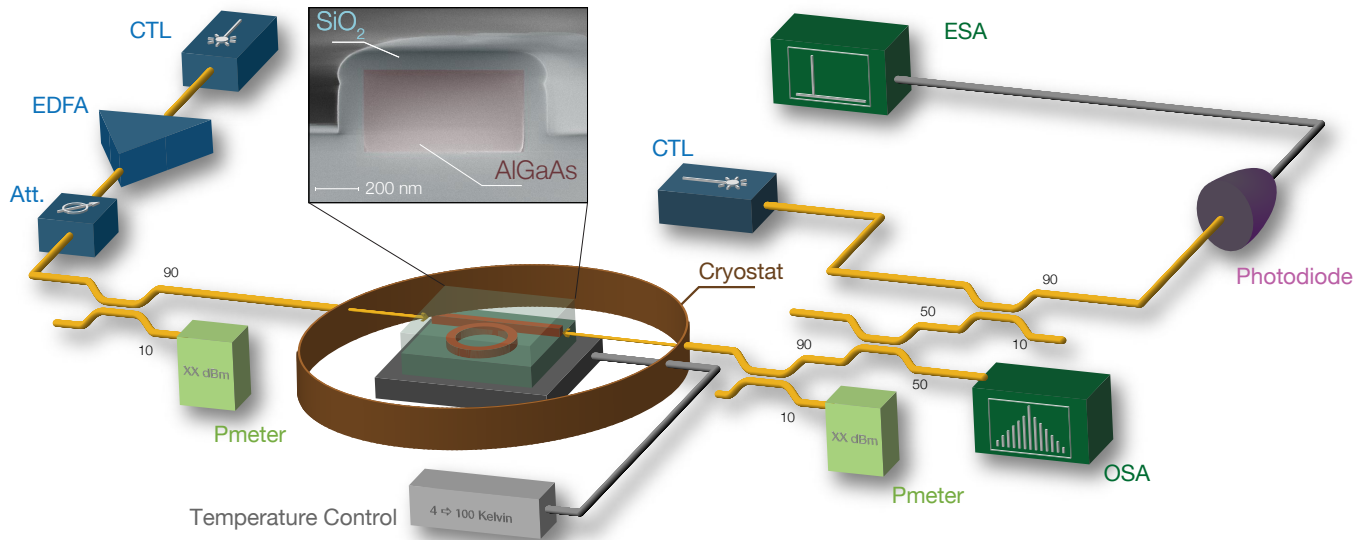


Figure 1. Experimental setup for generating a DKS in an AlGaAs-on-insulator microring resonator, where the sample is placed on top of a temperature-controlled mount inside a closed-cycle cryostat to modify the resonator's thermorefractive coefficient and achieve conditions favorable for DKS generation. The soliton is generated by manually tuning the frequency of the CTL pump laser, while the beat note measurement is performed using a second CTL laser. CTL: Continuous Tunable Laser, EDFA: Erbium Doped Fiber Amplifier, Pmeter: Power Meter, OSA: Optical Spectra Analyzer, ESA: Electrical Spectra Analyzer

First, we measure the shift of the resonances with temperature (T) to extract the thermorefractive coefficient $\partial n/\partial T$, where we probe the frequency shift of a resonance - the one which will be further pumped to generate the soliton frequency comb around 191.4 THz

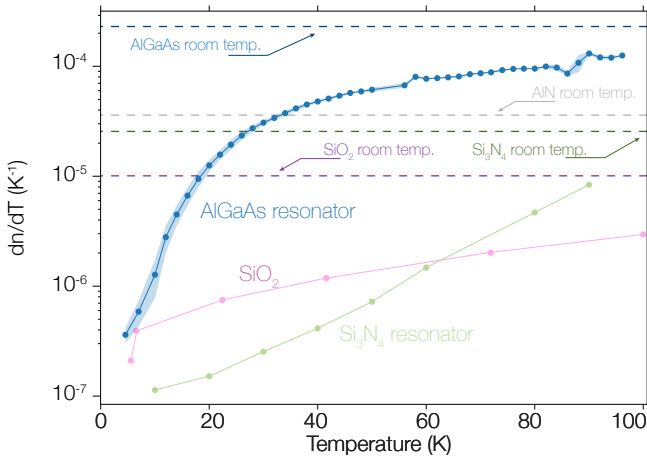


Figure 2. Measured thermorefractive coefficient $\partial n/\partial T$ versus T for the AlGaAs resonator (blue), Si₃N₄ resonator from ref. [27] (green), SiO₂ from ref. [28] (purple) and the room- T values for AlGaAs (dashed blue line) from ref. [29], Si₃N₄ (dashed green line) from ref. [27], and AlN (dashed grey line) from ref. [30]. The light blue area shows a range of $\partial n/\partial T$ values for the AlGaAs resonator if the sample temperature differs from the sample holder by up to ± 1 K.

- while changing the temperature of the sample mount from 7 K to 96 K. We do not observe significant change in either the coupling Q (average $\bar{Q}_c = 850 \times 10^3$) or the intrinsic Q (average $\bar{Q}_i = 575 \times 10^3$), as shown in Supplementary S-1. We believe that the resonator is limited by scattering losses and because the microring is pumped far from its band-edge, we cannot draw conclusions about a potential change of absorption due to temperature-induced band-gap modification. In order to retrieve the temperature dependence of dN/dT from the measured frequency shift, we first calculate $\frac{\partial \nu}{\partial n} = -55.98$ THz from an eigenmode solver, where ν is the eigenfrequency, and n is the refractive index of the AlGaAs, with the assumption that any variation in the refractive index of SiO₂ has little effect on the resonance frequency due to its small value and the large modal confinement within the AlGaAs layer (see Supplementary Material S-2). We then retrieve $\partial n/\partial T$ as $\frac{\partial n}{\partial T} = \frac{\partial \nu}{\partial T} \left(\frac{\partial \nu}{\partial n} \right)^{-1}$, with the results displayed in Fig. 2. It is important to note that we disregard thermal expansion as a potential source of a temperature-dependent resonance frequency shift, given its comparatively small expected value (near 10^{-7} K⁻¹), as reported in the literature [31].

The results of the measurements in Fig. 2 show that in addition to a nearly 100 times higher thermorefractive coefficient than Si₃N₄ and SiO₂ between 30 K and 60 K, the slope of $\partial n/\partial T$ ($\partial^2 n/\partial T^2$) for the AlGaAs system is quite large, as evidenced by an order of magnitude change in the range between $7 \text{ K} < T < 20 \text{ K}$. This suggests a more limited pump power and temperature

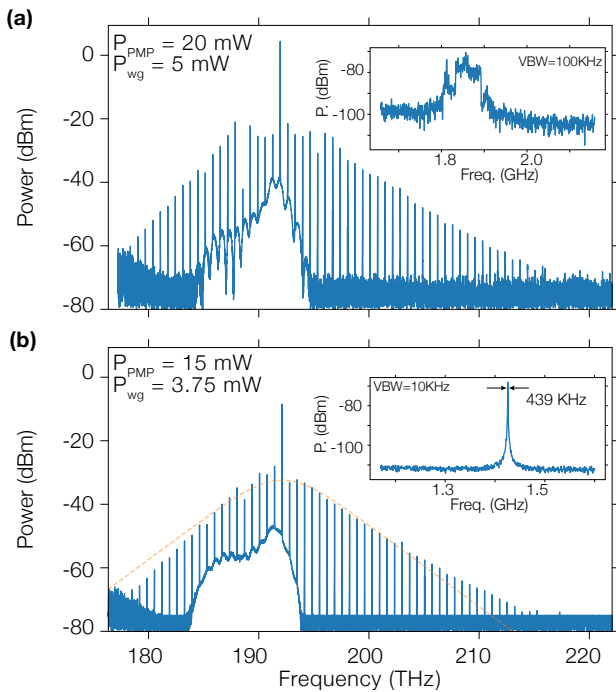


Figure 3. (a) MI comb spectrum for the resonator pumped at 15 mW in-waveguide power. (b) Single soliton spectrum when pumped at 4.3 mW in-waveguide power. Insets display beat note spectra acquired through interference of the comb tooth closest to 197 THz with a CW laser. These spectra are taken from DC to 6.8 GHz; the displayed data are zoomed in on the region of interest.

window for soliton accessibility under slow pump frequency tuning in AlGaAs than in Si₃N₄ [27].

In Fig. 3 we examine comb generation by pumping the resonator at $f_{\text{pmp}} = 191$ THz and by increasing the pump power to the few mW level. When the pump power is too high (in-waveguide power > 5 mW), only modulation instability (M.I.) states are observable, resulting in a comb spectrum that significantly differs from the sech^2 envelope expected for a soliton state. This is consistent with the broad beat note (inset to Fig. 3(a)) obtained through interference of the comb and a stabilized tunable laser near 197 THz. In contrast, for an in-waveguide power between 3 mW and 5 mW, the resulting comb spectrum (Fig. 3(b)) is significantly different from the M.I. one, and follows the expected sech^2 envelope. Furthermore, the beat note measurement (inset to Fig. 3(b)) shows a single narrow peak with significantly reduced noise floor relative to the M.I. state. This data, taken together, is indicative of stable access to a DKS state. The limited power window over which soliton states are adiabatically accessible appear to be strongly linked to the thermal properties of the system. Indeed, Al_{0.2}Ga_{0.8}As presents a relatively good thermal conductivity ($k_{\text{AlGaAs}} = 62.2 \text{ W}\cdot\text{m}^{-1}\cdot\text{K}^{-1}$ [32]), and is about a factor of 2 away from that of Si₃N₄

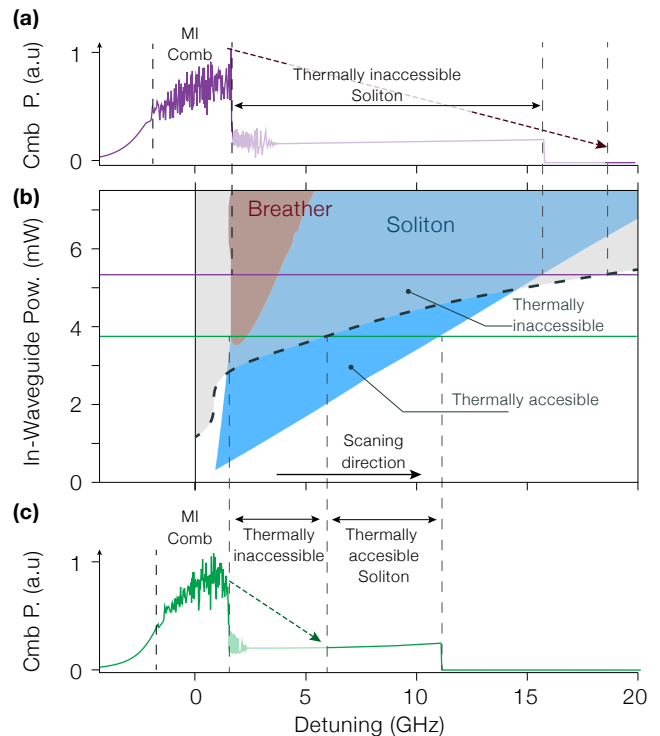


Figure 4. Soliton accessibility diagram highlighting the impact of the large gradient of the thermorefractive index between 4 K to 10 K. (a) When the pump power is too high, the soliton cannot be accessed through adiabatic tuning of the pump laser frequency, while when the power is sufficiently low, the soliton exists for detuning beyond the thermally inaccessible region. Panel (b) shows the soliton region (blue) computed from the Lugiato-Lefever equation including only Kerr dynamics, while the solution to a thermal model is plotted at a dashed black line. From this, the thermally accessible and inaccessible regions can be determined as indicated. In this figure, these regions are qualitatively defined, highlighting the crux of the experimental observations, but full quantitative detail is not achieved due to uncertainties in parameters that enter into the thermal model. The purple and green lines correspond to panels a and c, respectively, and are placed at their corresponding pump powers.

($k_{\text{Si}_3\text{N}_4} = 30 \text{ W}\cdot\text{m}^{-1}\cdot\text{K}^{-1}$ [17]). However, the microring in this study is being embedded within SiO₂ which is a thermal insulator ($k_{\text{SiO}_2} \simeq 1 \text{ W}\cdot\text{m}^{-1}\cdot\text{K}^{-1}$ [33]).

As a result, the temperature of the resonator can increase by a few degrees once a sufficiently large circulating power is reached. This relatively small increase of resonator temperature due to the pump will result in a large increase of the thermorefractive coefficient, resulting in a soliton state that is no longer thermally accessible. Fig. 4(b) summarizes this physical picture in a qualitative way (uncertainty in various quantities, such as the resonator absorption rate and heat capacity, preclude a fully quantitative description). In this figure, the soliton existence region within the 2D landscape of in-waveguide pump power and pump laser detuning from the cavity mode has been computed using

the steady-state Lugiato-Lefever equation through the *pyLLE* software [34], which only includes Kerr-mediated effects. Here, we have defined detuning as positive when the laser is on the red-detuned side of the cavity (i.e., at lower frequency). Thermal accessibility is addressed by a secondary equation as described in ref. [35], and is directly proportional to the thermorefractive index. Its solution is depicted by the black dashed line in Fig. 4(b). If the pump power is low enough, for example, corresponding to the horizontal green line in Fig. 4(b), $\partial n/\partial T$ is low enough, and the soliton existence window extends in laser detuning beyond the thermally inaccessible region and can be accessed adiabatically through slow frequency tuning of the pump (Fig. 4(c)). However, when the pump power is too high (purple horizontal line in Fig. 4(b)), the soliton existence window lies entirely within a thermally inaccessible region and can not be accessed adiabatically (Fig. 4(a)), resulting solely in the observation

of MI states.

In conclusion, we have demonstrated stable DKS operation in a III-V microring resonator. This has been realized by reducing its thermorefractive coefficient by more than two orders of magnitude through operation at cryogenic temperature. We further show that due to the large gradient of the thermorefractive coefficient between 4 K and 20 K, the pump power window over which soliton states are thermally accessible is limited. Our results show that thermorefractive effects have been the main limitation to soliton accessibility at room temperature, and point to the importance of minimizing optical absorption for realizing straightforward room-temperature access to DKSs in the future.

Acknowledgments. The authors acknowledge support from the DARPA DODOS program. G.M and K.S. thank Alfredo de Rossi for fruitful discussions.

-
- [1] T. J. Kippenberg, A. L. Gaeta, M. Lipson, and M. L. Gorodetsky, Dissipative Kerr solitons in optical microresonators, *Science* **361** (2018).
- [2] A. D. Ludlow, M. M. Boyd, J. Ye, E. Peik, and P. O. Schmidt, Optical atomic clocks, *Reviews of Modern Physics* **87**, 637 701 (2015).
- [3] T. E. Drake, T. C. Briles, J. R. Stone, D. T. Spencer, D. R. Carlson, D. D. Hickstein, Q. Li, D. Westly, K. Srinivasan, S. A. Diddams, and S. B. Papp, Terahertz-rate kerr-microresonator optical clockwork, *Phys. Rev. X* **9**, 031023 (2019).
- [4] N. Picqué and T. W. Hänsch, Frequency comb spectroscopy, *Nature Photonics* **13**, 146 (2019).
- [5] M.-G. Suh and K. J. Vahala, Soliton microcomb range measurement, *Science* **359**, 884 (2018).
- [6] X. Yi, Q.-F. Yang, K. Y. Yang, M.-G. Suh, and K. Vahala, Soliton frequency comb at microwave rates in a high-Q silica microresonator, *Optica* **2**, 1078 1078 (2015).
- [7] K. Saha, Y. Okawachi, B. Shim, J. S. Levy, R. Salem, A. R. Johnson, M. A. Foster, M. R. E. Lamont, M. Lipson, and A. L. Gaeta, Modelocking and femtosecond pulse generation in chip-based frequency combs, *Opt. Express* **21**, 1335 (2013).
- [8] T. Herr, V. Brasch, J. D. Jost, C. Y. Wang, N. M. Kondratiev, M. L. Gorodetsky, and T. J. Kippenberg, Temporal solitons in optical microresonators, *Nat. Photonics* **8**, 145 (2014).
- [9] X. Liu, A. W. Bruch, J. Lu, Z. Gong, J. B. Surya, L. Zhang, J. Wang, J. Yan, and H. X. Tang, Beyond 100 THz-spanning ultraviolet frequency combs in a non-centrosymmetric crystalline waveguide, *Nature Communications* **10**, 2971 (2019).
- [10] Z. Gong, A. Bruch, M. Shen, X. Guo, H. Jung, L. Fan, X. Liu, L. Zhang, J. Wang, J. Li, J. Yan, and H. X. Tang, High-fidelity cavity soliton generation in crystalline all micro-ring resonators, *Opt. Lett.* **43**, 4366 (2018).
- [11] Y. He, Q.-F. Yang, J. Ling, R. Luo, H. Liang, M. Li, B. Shen, H. Wang, K. Vahala, and Q. Lin, Self-starting bi-chromatic LiNbO₃ soliton microcomb, *Optica* **6**, 1138 (2019).
- [12] M. Pu, L. Ottaviano, E. Semenova, and K. Yvind, Efficient frequency comb generation in algaas-on-insulator, *Optica* **3**, 823 (2016).
- [13] L. Chang, W. Xie, H. Shu, Q. Yang, B. Shen, A. Boes, J. D. Peters, W. Jin, S. Liu, G. Moille, *et al.*, Ultra-efficient frequency comb generation in algaas-on-insulator microresonators, *Nature communications* **11**, 1331 (2020).
- [14] D. J. Wilson, K. Schneider, S. Hnl, M. Anderson, Y. Baumgartner, L. Czornomaz, T. J. Kippenberg, and P. Seidler, Integrated gallium phosphide nonlinear photonics, *Nature Photonics* , 5762 (2020).
- [15] S. T. Ho, C. E. Socolich, M. N. Islam, W. S. Hobson, A. F. J. Levi, and R. E. Slusher, Large nonlinear phase shifts in low-loss Al_xGa_{1-x}As waveguides near half-gap, *Applied Physics Letters* **59**, 2558 (1991).
- [16] J. S. Aitchison, D. C. Hutchings, J. U. Kang, G. I. Stegeman, and A. Villeneuve, The nonlinear optical properties of algaas at the half band gap, *IEEE Journal of Quantum Electronics* **33**, 341 (1997).
- [17] K. Ikeda, R. E. Saperstein, N. Alic, and Y. Fainman, Thermal and kerr nonlinear properties of plasma-deposited silicon nitride/silicon dioxide waveguides, *Optics express* **16**, 12987 (2008).
- [18] H. Jung, C. Xiong, K. Y. Fong, X. Zhang, and H. X. Tang, Optical frequency comb generation from aluminum nitride microring resonator, *Opt. Lett.* **38**, 2810 (2013).
- [19] G. Stegeman, A. Villeneuve, J. Kang, J. Aitchison, C. Ironside, K. Al-Hemyari, C. Yang, C.-H. Lin, H.-H. Lin, G. Kennedy, R. Grant, and W. Sibbett, Algaas below half bandgap: the silicon of nonlinear optical materials, *Journal of Nonlinear Optical Physics & Materials* **03**, 347 (1994).
- [20] F. Capasso, Band-gap engineering: From physics and materials to new semiconductor devices, *Science* **235**, 172 (1987).
- [21] P. Colman, C. Husko, S. Combrié, I. Sagnes, C. Wong, and A. De Rossi, Temporal solitons and pulse compression in photonic crystal waveguides, *Nature Photonics* **4**, 862 (2010).

- [22] C. Husko, A. De Rossi, S. Combrié, Q. V. Tran, F. Raineri, and C. W. Wong, Ultrafast all-optical modulation in GaAs photonic crystal cavities, *Applied Physics Letters* **94**, 021111 (2009).
- [23] G. Moille, S. Combrié, L. Morgenroth, G. Lehoucq, F. Neuilly, B. Hu, D. Decoster, and A. de Rossi, Integrated all-optical switch with 10 ps time resolution enabled by ALD, *Laser & Photonics Reviews* **10**, 409 (2016).
- [24] A. Martin, G. Moille, S. Combrié, G. Lehoucq, T. Debuisschert, J. Lian, S. Sokolov, A. P. Mosk, and A. de Rossi, Triply-resonant continuous wave parametric source with a microwatt pump, in *Conference on Lasers and Electro-Optics (CLEO)* (2016) pp. 1–2.
- [25] R. J. Deri, E. Kapon, and L. M. Schiavone, Scattering in lowloss gaas/algaas rib waveguides, *Applied Physics Letters* **51**, 789 (1987).
- [26] V. Van, P. P. Absil, J. V. Hryniewicz, and P.-T. Ho, Propagation loss in single-mode gaas-algaas microring resonators: Measurement and model, *J. Lightwave Technol.* **19**, 1734 (2001).
- [27] G. Moille, X. Lu, A. Rao, Q. Li, D. A. Westly, L. Ranzani, S. B. Papp, M. Soltani, and K. Srinivasan, Kerr-microresonator soliton frequency combs at cryogenic temperatures, *Phys. Rev. Applied* **12**, 034057 (2019).
- [28] A. W. Elshaari, I. E. Zadeh, K. D. Jons, and V. Zwiller, Thermo-Optic Characterization of Silicon Nitride Resonators for Cryogenic Photonic Circuits, *IEEE Photonics Journal* **8**, 1 (2016).
- [29] E. A. Camargo, H. M. Chong, and M. Richard, 2d photonic crystal thermo-optic switch based on algaas/gaas epitaxial structure, *Optics Express* **12**, 588 (2004).
- [30] N. Watanabe, T. Kimoto, and J. Suda, Thermo-optic coefficients of 4h-SiC, GaN, and AlN for ultraviolet to infrared regions up to 500 °C, *Japanese Journal of Applied Physics* **51**, 112101 (2012).
- [31] S. I. Novikova, *Sov. Phys. Solid State* **3**, 129 (1961).
- [32] M. A. Fromowitz, Thermal conductivity of $\text{Ga}_{1-x}\text{Al}_x\text{As}$ alloys, *Journal of Applied Physics* **44**, 1292 (1973).
- [33] T. Yamane, N. Nagai, S.-i. Katayama, and M. Todoki, Measurement of thermal conductivity of silicon dioxide thin films using a *3omega* method, *Journal of Applied Physics* **91**, 9772 (2002).
- [34] G. Moille, Q. Li, X. Lu, and K. Srinivasan, pyLLE: a Fast and User Friendly Lugiato-Lefever Equation Solver, *Journal of Research of National Institute of Standards and Technology* **124**, 124012 (2019).
- [35] Q. Li, T. C. Briles, D. A. Westly, T. E. Drake, J. R. Stone, B. R. Ilic, S. A. Diddams, S. B. Papp, and K. Srinivasan, Stably accessing octave-spanning microresonator frequency combs in the soliton regime, *Optica* **4**, 193 (2017).
- [36] M. Borselli, T. Johnson, and O. Painter, Beyond the Rayleigh scattering limit in high-Q silicon microdisks: theory and experiment, *Optics Express* **13**, 1515.

SUPPLEMENTARY MATERIAL

S-1. Linear Measurements

The linear measurements are performed using a wavemeter- and reference cell-based calibrated laser system, allowing retrieval of the resonance frequency of the mode of interest (see Fig. S1(a)) with ≈ 0.1 pm accuracy. Using a doublet fitting model [36], we determine the intrinsic and coupling quality factors of the resonant mode. We change the temperature of the sample holder by increment of 5 degrees, and the measured resonance frequency and extracted quality factors are shown in Fig. S1.

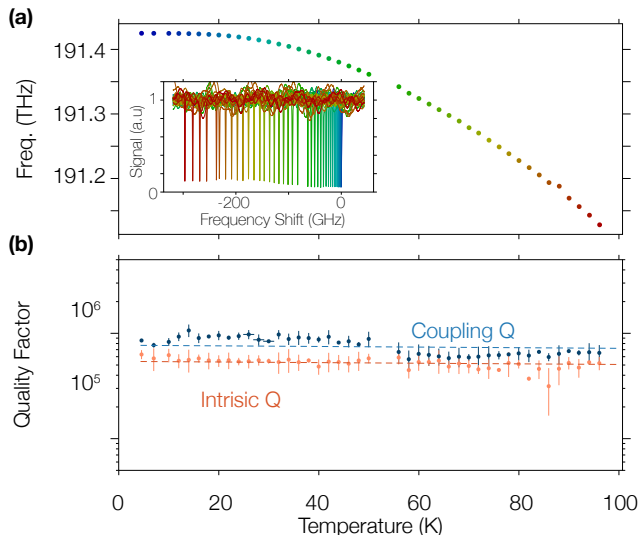


Figure S1. (a) Measurement of the shift of the resonance frequency of the microring mode used to generate a frequency comb. The inset displays the resonance with the trace color corresponding to the temperature. (b) Coupling quality factor (blue) and intrinsic quality factor (orange) of the pumped resonance. The uncertainty due to the fit is represented by the vertical bar and corresponds to one standard deviation.

S-2. Determination of Thermo-refractive index

The thermo-refractive index of the system can be retrieved using the formula $\frac{\partial n}{\partial T} = \frac{\partial \nu}{\partial T} \left(\frac{\partial \nu}{\partial n} \right)^{-1}$, where $\frac{\partial \nu}{\partial T}$ is obtained using the results presented in Fig. S1(a), while $\frac{\partial \nu}{\partial n}$ is computed using an eigenfrequency solver. Here, we make two assumptions. First, according to the literature, the thermo-refractive coefficient of SiO₂ is low (between $5 \times 10^{-7} \text{ K}^{-1}$ to $1 \times 10^{-6} \text{ K}^{-1}$) and its variation is negligible within the temperature range of interest. Secondly, because the mode is highly confined within the AlGaAs ring resonator (confirmed by comparing the mode area ($A_{\text{mode}} = 1.94 \times 10^{-13} \text{ m}^2$) to the ring resonator cross-section area ($A_{\text{ring}} = 2.6 \times 10^{-13} \text{ m}^2$), the influence of the SiO₂ cladding and underlying substrate are negligible. Hence, in the eigenfrequency simulation, we vary the refractive index of the AlGaAs and obtain $\frac{\partial \nu}{\partial n}$ from linear fit (Fig. S2)

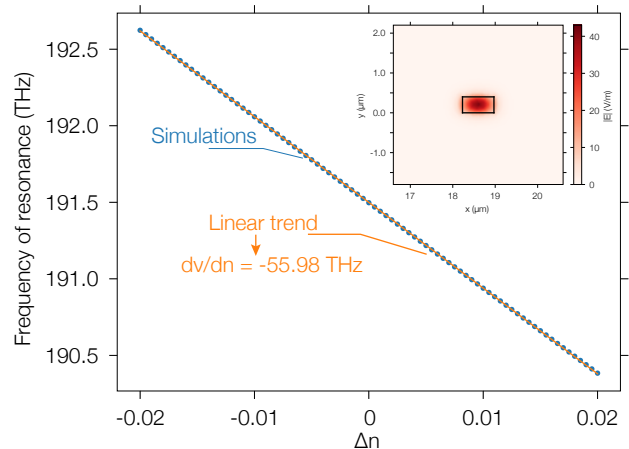


Figure S2. Simulation of the shift of the resonance frequency with a small change of the refractive index of the microring core material Δn (blue dots). The linear fit used to extract $\frac{\partial \nu}{\partial n}$ is represented through the orange line. The inset represent the electric field of the mode of interest